Chemical Science

ROYAL SOCIETY OF CHEMISTRY

EDGE ARTICLE

View Article Online
View Journal | View Issue



Cite this: *Chem. Sci.*, 2020, **11**, 2926

All publication charges for this article have been paid for by the Royal Society of Chemistry

# A clustering-triggered emission strategy for tunable multicolor persistent phosphorescence†

Qing Zhou, Tianjia Yang, Zihao Zhong, Fahmeeda Kausar, Ziyi Wang, Yongming Zhang* and Wang Zhang Yuan *

Received 24th December 2019
Accepted 10th February 2020

DOI: 10.1039/c9sc06518k

rsc.li/chemical-science

A clustering-triggered emission (CTE) strategy, namely the formation of heterogeneous clustered chromophores and conformation rigidification, for achieving tunable multicolor phosphorescence in single-component compounds is proposed. Non-conventional luminophores comprising just oxygen functionalities and free of π-bonding, *i.e.*, D-(+)-xylose (D-Xyl), pentaerythritol (PER), D-fructose (D-Fru) and D-galactose (D-Gal), were adopted as a simple model system with an explicit structure and molecular packing to address the hypothesis. Their concentrated solutions and crystals at 77 K or under ambient conditions demonstrate remarkable multicolor phosphorescence afterglows in response to varying excitation wavelengths, because of the formation of diverse oxygen clusters with sufficiently rigid conformations. The intra- and inter-molecular O···O interactions were definitely illustrated by both single crystal structure analysis and theoretical calculations. These findings shed new light on the origin and simple achievement of tunable multicolor phosphorescence in single-component pure organics, and in turn, have strong implications for the emission mechanism of non-conventional luminophores.



## Introduction

Currently, the development of smart luminescent materials with tunable multicolor emission upon external stimuli, such as temperature, light, electric/magnetic field, excitation intensity and pressure, is receiving increasing attention because of their unique photophysical properties and potential applications in information encryption, visual detection of UV lights, anti-counterfeiting, sensing and bioassays.[1–8] Thus far, despite the fact that multicolor luminescence has been successfully achieved through the modulation of crystallinity, molecular conformation/packing and composition of the compounds, or the combination of different emitters,[5–13] it remains challenging to realize the tunability of persistent phosphorescence in pure organic single-component systems,[14–20] particularly in single crystals.[14] While there is growing interest in the achievement of pure organic persistent room temperature phosphorescence (p-RTP),[21–27] little attention has been given to its tunability,[14–20] presumably because of the high susceptibility of triplets[28–38] and the difficulty in the construction of diverse triplet emissive populations.

Very recently, tunable multicolor persistent phosphorescence from pure organics has been observed in certain nonaromatic luminophores,[18–20] aromatic crystals[14] and ionized or doped polymers,[15–17] at cryogenic temperatures (*i.e.*, 77 K) and/or even under ambient conditions. For example, Huang and co-workers demonstrated tunable p-RTP in 2,4,6-trimethoxy-1,3,5-triazine (TMOT) crystals,[14] and Zhao *et al.* reported a tunable afterglow from blue to red by tuning the aggregation state of pyrene derivatives in poly(vinyl alcohol) (PVA) films.[17] Meanwhile, tunable cryogenic phosphorescence was observed from concentrated solutions of sodium alginate (SA),[18] poly(acrylic acid) (PAA),[19] poly(acrylamide) (PAM)[19] and natural proteins,[20] the emission colors of which generally changed from blue to green with the variation in the excitation wavelengths ($\lambda_{ex}$s) from 312 to 365 nm at 77 K, because of the presence of multiple emissive species.[18–20] Furthermore, bovine serum albumin (BSA)[20] and ε-poly-L-lysine (ε-PLL)[39] have even been shown to exhibit $\lambda_{ex}$-dependent p-RTP. Despite these exciting advances, the understanding of the origination of such emissions, and moreover, the design rationale, remain elusive. For example, monomer and excimer phosphorescence were ascribed to the occurrence of tunable p-RTP in the TMOT system, where planar conformation was believed to play an important role in guaranteeing the formation of H-aggregates,[14] whereas diverse clustered chromophores were thought to be the origin of the non-conventional luminophores.[18–20,39]

*School of Chemistry and Chemical Engineering, Shanghai Key Lab of Electrical Insulation and Thermal Aging, Shanghai Electrochemical Energy Devices Research Center, Shanghai Jiao Tong University, Shanghai 200240, China. E-mail: ymzhang@sjtu.edu.cn; wzhyuan@sjtu.edu.cn*

† Electronic supplementary information (ESI) available: Detailed experimental procedures, characterization data; photophysical data and chemical structure of the compounds. CCDC 1934968 (D-Xyl), 1934967 (PER), 1934969 (D-Fru) and 1934964 (D-Gal). For ESI and crystallographic data in CIF or other electronic format see DOI: 10.1039/c9sc06518k

Taking together all the preceding reports, it is clear that the presence of multiple emissive centers alongside rigid conformations are necessary for tunable multicolor phosphorescence.[14–20] These features, fortunately, are exactly the two key points required for achieving unusual luminescence from non-conventional luminogens devoid of classic conjugates.[39–43] On account of the less effective delocalization of the subunits, individual non-conventional luminophores are virtually non-emissive.[39,44–49] The clustering-triggered emission (CTE) mechanism was proposed to rationalize such photophysical properties.[18–20,39,50] In this scenario, the clustering of non-conventional chromophores, with lone pairs (n) and/or π electrons to yield clustered chromophores with varying extended electron delocalization, are responsible for the $\lambda_{ex}$-dependent emission (Fig. 1a).[18–20,39,43]

Inspired by the heterogeneous clustered chromophores of non-conventional luminophores, and considering the prompting effect of heteroatoms on the spin–orbit coupling (SOC), it is speculated that the CTE strategy is highly promising for tunable multicolor persistent phosphorescence (Fig. 1a and b). Although several atypical luminescent polymers have shown $\lambda_{ex}$-dependent phosphorescence,[15,18–20] their complicated chain entanglement makes it difficult to gain a clear picture of the electronic interactions among the subunits. Despite the fact that their molecular counterparts[51,52] can provide more explicit conformations and molecular packing, there have been no reports concerning their tunable afterglows. To further the understanding of the origin of tunable persistent phosphorescence, it is urgently needed to establish a simple molecular model system. To simplify the interference of different subunits, we here chose luminophores such as those bearing just oxygen functionalities, namely pentaerythritol (PER), D-(+)-xylose (D-Xyl), D-fructose (D-Fru) and D-galactose (D-Gal) (Fig. S1, S2 and Table S1, ESI†). They are ready to form crystals comprising oxygen clusters, which would also allow access to structural diversity through electronic communications.[53–55]

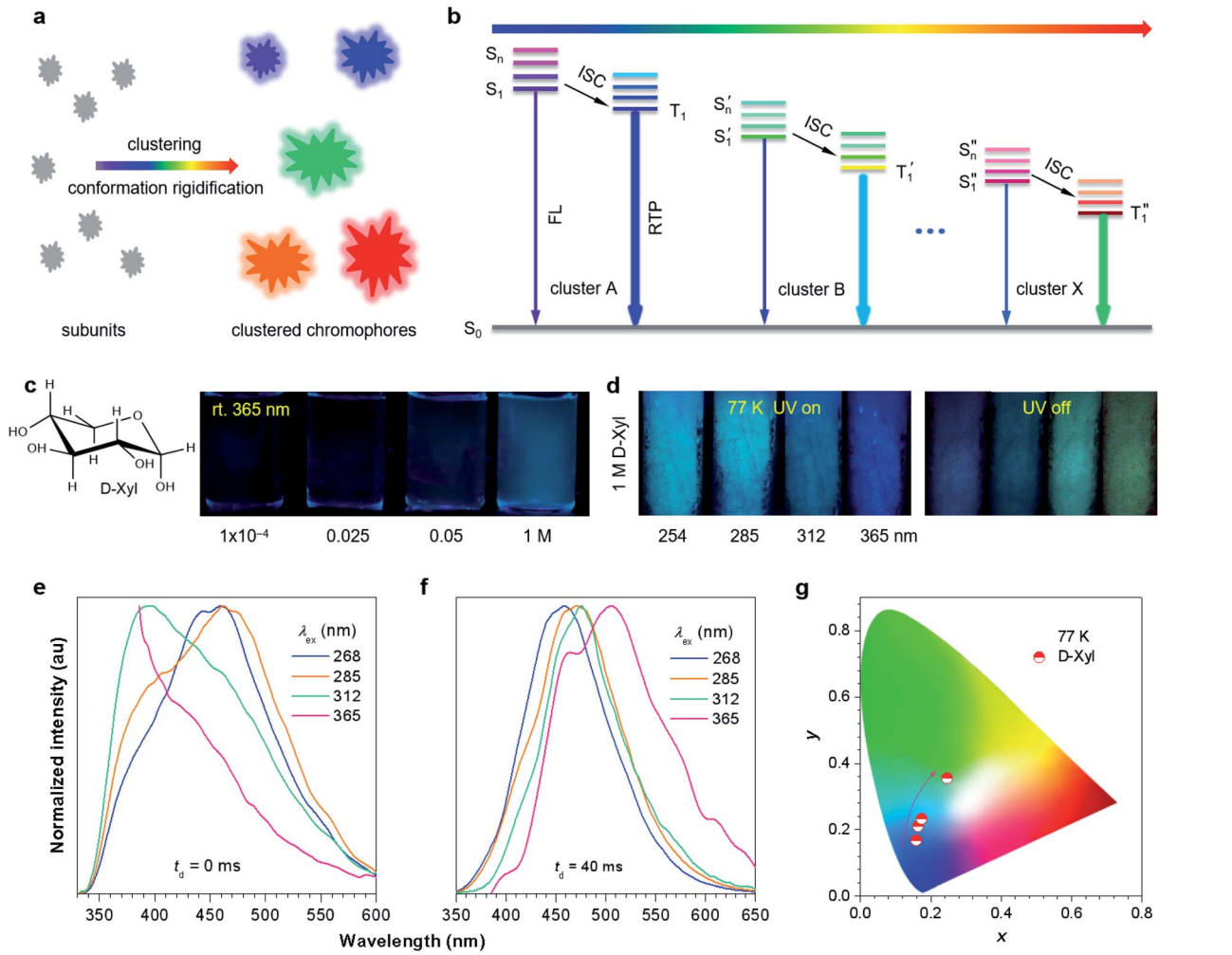


Fig. 1 (a) Schematic illustration of the CTE mechanism of non-conventional luminophores. (b) Jablonski diagram for the demonstration of color tunable luminescence in non-conventional luminophores. (c) Photographs of different aqueous D-Xyl solutions taken under 365 nm UV light at room temperature. (d) Photographs of 1 M D-Xyl solution taken at 77 K under various wavelengths of UV light or after stopping the UV irradiation. (e and f) Emission spectra of 1 M D-Xyl solution at 77 K with a $t_d$ of (e) 0 ms and (f) 40 ms. (g) CIE coordinate diagram of the cryogenic phosphorescence of 1 M D-Xyl with $\lambda_{ex}$ changing from 268 to 365 nm.

Furthermore, multiple hydrogen bonds are beneficial for the formation of oxygen clusters with rigid conformations.[51,52] Fortunately, even without any π segments, all the crystals demonstrated tunable multicolor p-RTP and more obvious tunability was achieved for them and their concentrated solutions at 77 K, thus confirming the speculation. Notably, although the triboluminescence of sugars has been reported, their photoluminescence (PL) behavior and mechanism have not yet been discussed in detail.[56,57] The results given here also provide insights into the origin of the tunable phosphorescence in single-component systems and advance the understanding of the emission mechanism of non-conventional luminophores, including sugars.

## Results and discussion

For comparison, distilled glycerol (Gly) was first investigated as control. Liquid Gly is non-emissive at room temperature, whereas it is highly luminescent at 77 K with tunable afterglows from blue to light green by varying the $\lambda_{ex}$ (Fig. S3, ESI†). Encouraged by these results, it was speculated that heterogeneous oxygen clusters with sufficiently rigidified conformations in solids might provide tunable p-RTP. To verify it, D-Xyl, a saccharide with a much higher molecular weight and more hydroxyls than Gly (Fig. 1c) was investigated, and which would produce more effective hydrogen bonds to stiffen the molecular conformations. Aqueous D-Xyl solutions exhibited concentration enhanced emission and multiple emission maxima (Fig. 1c and S4, ESI†), which are explainable in terms of the CTE mechanism (Fig. S5, ESI†),[43,50] considering the formation of different oxygen clusters and conformation rigidification.[43,50,53–55] Furthermore, the presence of diverse oxygen clusters was also validated by looking at the various lifetimes at different maxima (Fig. S6 and Table S2, ESI†). Upon freezing to 77 K, with different $\lambda_{ex}$s from 254 to 365 nm, the emission color of the concentrated D-Xyl solution (1 M) changed from cyan to blue (Fig. 1d), which originated from the ratiometric variation among the emission maxima/shoulders at 393, 443 and 462 nm (Fig. 1e). Moreover, after stopping the irradiations, bright afterglows with tunable colors from blue to greenish-yellow were observed (Fig. 1d). These afterglows corresponded to the cryogenic phosphorescence, whose spectra were red-shifted with increasing $\lambda_{ex}$ from 268 to 365 nm (Fig. 1f), further verifying the coexistence of diverse oxygen clusters. The Commission International de l'Eclairage (CIE) coordinates, which were derived from the PL spectra, were calculated and are shown in Fig. 1g, which again verifies the variation of the phosphorescence colors as observed.

Considering the more rigidified conformations at crystals than in solutions, D-Xyl crystals were expected to possess tunable multicolor p-RTP at ambient conditions. Thus, the crystal emission was checked next. Comparing the PL efficiency ($\Phi$) of 1 M solutions (0.6%, Table 1), with that of crystals, the crystals show a much higher efficiency (2.2%, Table 1), because of the further rigidification of the oxygen clusters. From being virtually non-luminescent in dilute solutions (*i.e.*, $10^{-4}$ M, $\Phi = 0$) to brightly emissive in crystals, D-Xyl exhibited apparent aggregation-induced emission (AIE) characteristics.[58] Despite resembling blue PL under different $\lambda_{ex}$s (Fig. 2a, upper set of images), the presence of multiple maxima with varying lifetimes of the prompt emissions (Fig. 2b and S7, ESI†) implied that there were concurrent diverse emissive species. Furthermore, as expected, distinct emission colors of blue, cyan, bluish-green and green were visualized after stopping the UV light of 254, 285, 312 and 365 nm (Fig. 2a and Video S1, ESI†), respectively. Such afterglows were ascribed to the p-RTP emissions, as evidenced by their long lifetimes ($\langle\tau\rangle_p$) ranging from 274 to 739 ms (Fig. 2c and Table S3, ESI†). To gain a deeper insight into such an intriguing color-tunable p-RTP, the excitation–phosphorescence mapping of the crystals was performed. As $\lambda_{ex}$ changed from 245 to 325 nm, the p-RTP emission correspondingly exhibited an obvious bathochromic shift from blue to green alongside the peak/shoulder varying from 435/475 to 525 nm (Fig. 2d). Such tunable p-RTP colors in response to the variation in $\lambda_{ex}$ are also illustrated in the CIE coordinate diagram (Fig. 2e), from which the color evolution from blue to green is noticed. Specifically, the p-RTP spectra ($t_d = 0.1$ ms) with $\lambda_{ex}$s of 255, 285 and 315 nm were peaking at 435/475, 510 and 525 nm (Fig. 2d), with CIE coordinates of (0.241, 0.257), (0.285, 0.456) and (0.311, 0.480) (Fig. 2e), respectively, which were highly consistent with the naked eye observation.

It was also noted that multiple maxima and/or broad full width at half maxima (FWHM) of greater than 116 nm (Fig. 2d) in the p-RTP spectra highly suggest the co-existence of varying emissive species even with a fixed $\lambda_{ex}$. This was supported by the different $\langle\tau\rangle_p$s at 435 and 475 nm with the same $\lambda_{ex}$ of 255 nm (Fig. 2c), as well as the multi-exponential decay profiles for each monitored wavelength (Table 1). To further understand the

Table 1 Photophysical data of the solutions and crystals of various compounds[a]

| | D-Xyl | PER | D-Fru | D-Gal |
|---|---|---|---|---|
| Samples | $\lambda_{ex,o}/\lambda_{em,o}/\Phi$ [nm]/[nm]/[%] | $\lambda_{ex,o}/\lambda_{em,o}/\Phi$ [nm]/[nm]/[%] | $\lambda_{ex,o}/\lambda_{em,o}/\Phi$ [nm]/[nm]/[%] | $\lambda_{ex,o}/\lambda_{em,o}/\Phi$ [nm]/[nm]/[%] |
| Solution[b] | 284/354/0.6 | 270/452/0.5 | 268/432/0.3 | 340/429/0.8 |
| Solution[c] | 284/321/0.0 | 270/302/0.0 | 268/301/0.0 | 340/387/0.0 |
| Crystal | 360/429/2.7 | 270/460/2.2 | 280/495/1.8 | 280/451/4.1 |

[a] $\lambda_{ex,o}$ = optimal excitation wavelength; $\lambda_{em,o}$ = optimal emission wavelength; $\Phi$ = quantum efficiency. [b] Concentration: 1 M (D-Xyl, D-Fru and D-Gal), 0.1 M (PER). [c] Concentration: $1 \times 10^{-4}$ M.

 

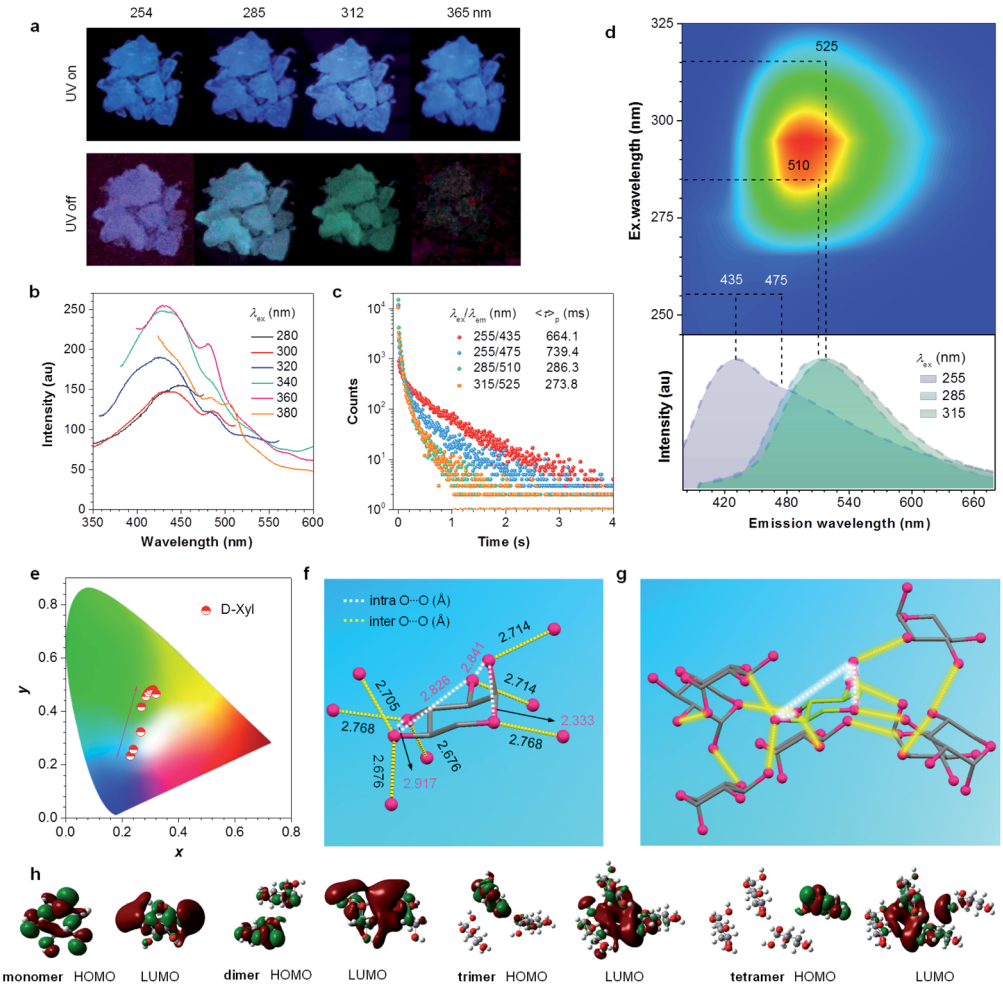


Fig. 2 (a) Photographs of D-Xyl crystals taken under various wavelengths of UV light or after stopping the irradiation at ambient conditions. (b) Prompt PL spectra of D-Xyl crystals with different $\lambda_{ex}$ values. (c) Decay profiles for D-Xyl crystals monitored at various emission wavelengths ($\lambda_{em}$s). (d) Excitation–p-RTP mapping and p-RTP spectra with different excitations ($t_d$ = 0.1 ms) for D-Xyl crystals. (e) Trajectory of tunable p-RTP colors, recorded by the change in the $\lambda_{ex}$ from 245 to 325 nm, in the CIE coordinate diagram. (f) Single crystal structure of D-Xyl with denoted intra- and inter-molecular O···O interactions. (g) Fragmental molecular packing of D-Xyl in crystals with denoted O···O short contacts. (h) HOMO and LUMO electron densities of monomer, dimer, trimer and tetramer of D-Xyl.

tunable p-RTP, the single crystal structure of D-Xyl was determined. Notably, besides H–O···H–O (1.781, 1.859, 1.955 Å), O–H···C–H (2.717, 2.808, 2.863 Å) and H–O···H–C (2.559, 2.690 Å) hydrogen bonds, intermolecular short dihydrogen bonds of O–H···H–O (2.343 Å), C–H···H–O (2.395 Å) and C–H···H–C (2.342 Å) were also present (Fig. S8, ESI†), which remarkably restricted the molecular motions, thus providing rigid conformations in the crystals. Moreover, abundant intramolecular (2.333, 2.826, 2.841, 2.917 Å) and intermolecular (2.676, 2.705, 2.714, 2.768 Å) O···O electronic interactions were found (Fig. 2f), whose distances were much shorter than the sum of the vdW radii (3.04 Å), thus leading to effective 3D through-space conjugation of the lone pairs (Fig. 2g). Furthermore, the clustering of oxygens enriched the energy levels and narrowed the energy gaps of diverse clustered chromophores, which would promote the spin–orbit coupling (SOC) and consequent intersystem crossing (ISC) transitions. Therefore, derived from these oxygen clusters with varying energy gaps, strikingly excitation-dependent multicolor p-RTP were readily observable while waiting for sufficiently rigidified conformations through effective intra- and inter-molecular interactions (Fig. 1b). To further understand the mechanism, the HOMO and LUMO electron densities of monomer, dimer, trimer and tetramer of D-Xyl were calculated (Fig. S9, ESI†). Although the results remain preliminary, the electron density distribution of the monomer clearly indicated the intramolecular O···O electron delocalization (Fig. 2h). In addition, the LUMO levels of other aggregates clearly illustrated the extended delocalization among the neighboring molecules in excited states (Fig. 2h), which agreed well with the postulated hypothesis. Because of the preceding results, more luminogens with tunable p-RTP were confidently explored using the CTE strategy. To check the universality of it, the PL properties of PER, D-Fru and D-Gal were studied further (Fig. 3a, S10–S13, ESI† and Table 1). Resembling D-Xyl, they all exhibited AIE characteristics, as shown by D-Gal (Fig. S10 and S12, ESI†). In addition, the PL

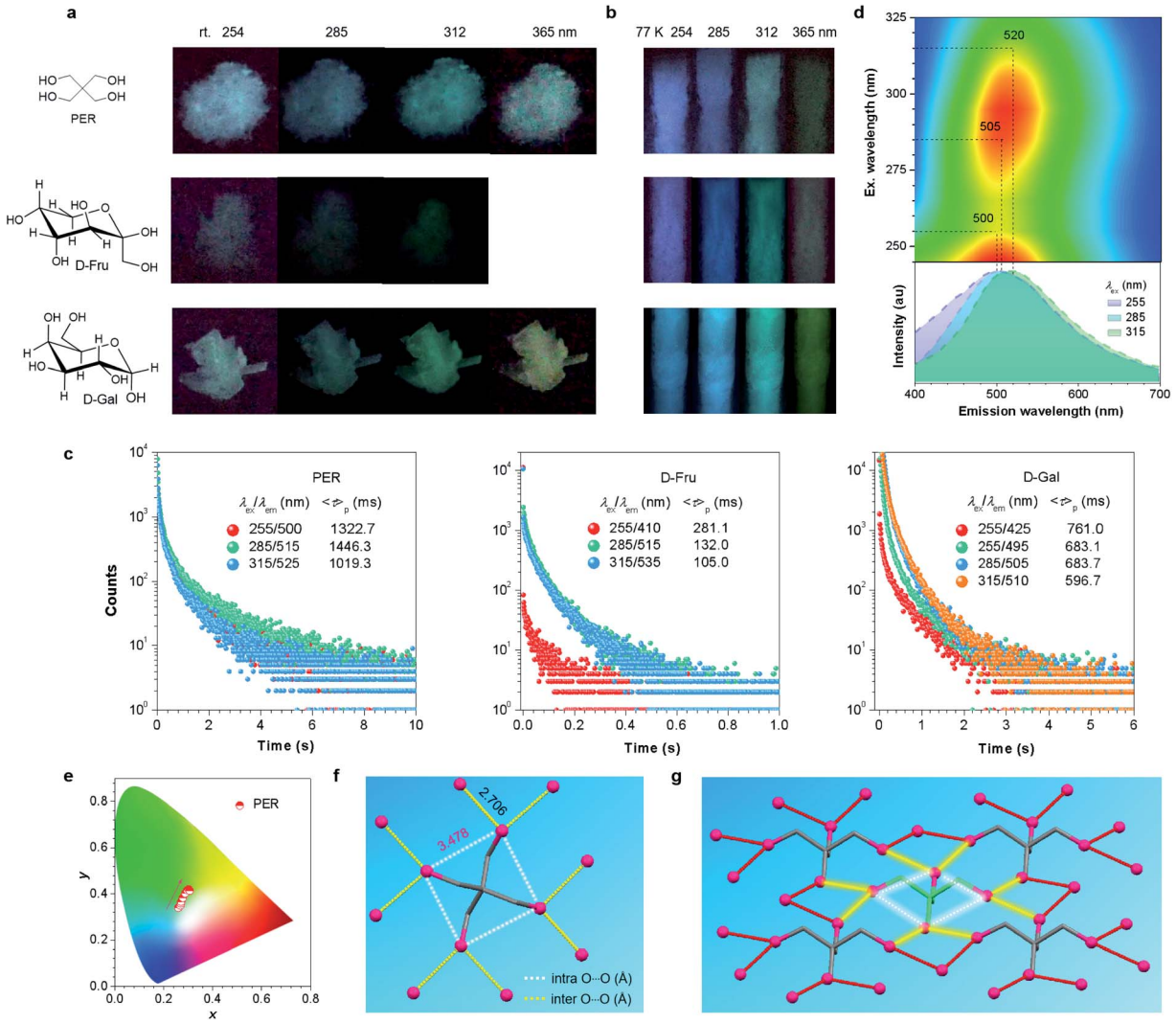


Fig. 3 (a) Photographs of the crystals of PER, D-Fru and D-Gal taken at room temperature after stopping UV irradiation at different wavelengths. (b) Photographs of concentrated aqueous solutions for PER (0.1 M), D-Fru (1 M) and D-Gal (1 M) taken at 77 K after stopping UV irradiation at different wavelengths. (c) Decay profiles of the crystals of PER, D-Fru and D-Gal monitored at varying $\lambda_{em}$s at room temperature (rt). (d) Excitation–p-RTP mapping and p-RTP spectra with different excitations ($t_d$ = 0.1 ms) for PER crystals. (e) Trajectory of tunable p-RTP colors of PER crystals, recorded as the change in the $\lambda_{ex}$ from 245 to 325 nm, in the CIE coordinate diagram. (f) Single crystal structure of PER with the intra- and intermolecular O···O interactions marked. (g) Fragmental molecular packing of PER in crystals with the O···O short contacts marked.

spectra of the crystals showed multiple maxima, which were associated with distinctive emission species (Fig. S13, ESI†). Although the observed p-RTP colors of their crystals did not vary considerably upon excitation with different $\lambda_{ex}$s, from greenish-white to yellow/greenish-yellow (Fig. 3a and Video S2, ESI†), those of the cryogenic phosphorescence of their concentrated solutions demonstrated more apparent tunability (Fig. 3b and S11, ESI†), which presumably originated from the more widespread distribution of oxygen clusters in solutions and immensely rigidified conformations at 77 K. Time-resolved measurement revealed long $\langle\tau\rangle_p$ values for the crystals, ranging from hundreds of microseconds to ~1.45 s (Fig. 3c), which were among the longest values for both aromatic[34,59–64] and non-conventional luminogens.[15,18–20,51] Meanwhile, the multiple decay components of p-RTP indicated the simultaneous contribution from an ensemble of emissive species within a heterogeneous population (Tables S4–S6, ESI†), which was consistent with their unstructured spectra and broad FWHM of >131 nm (Fig. 3d and S14, S15, ESI†). Thus, tunable p-RTP can be readily realized from these crystals by changing the $\lambda_{ex}$, which resulted in the formation of heterogeneous oxygen clusters.

Further excitation–phosphorescence mapping (Fig. 3d and S14, S15, ESI†) and the CIE coordinate diagrams (Fig. 3e and S14, S15, ESI†) clearly showed the peaks and color changes of p-RTP in response to the increasing $\lambda_{ex}$, thus verifying their tunability. Taking PER as an example, as the $\lambda_{ex}$ changed from 245 to 325 nm, the p-RTP maximum was red-shifted from 500 to 520 nm, which were all located in the green region (Fig. 3d). Meanwhile, their CIE coordinate diagram shows nearly linear

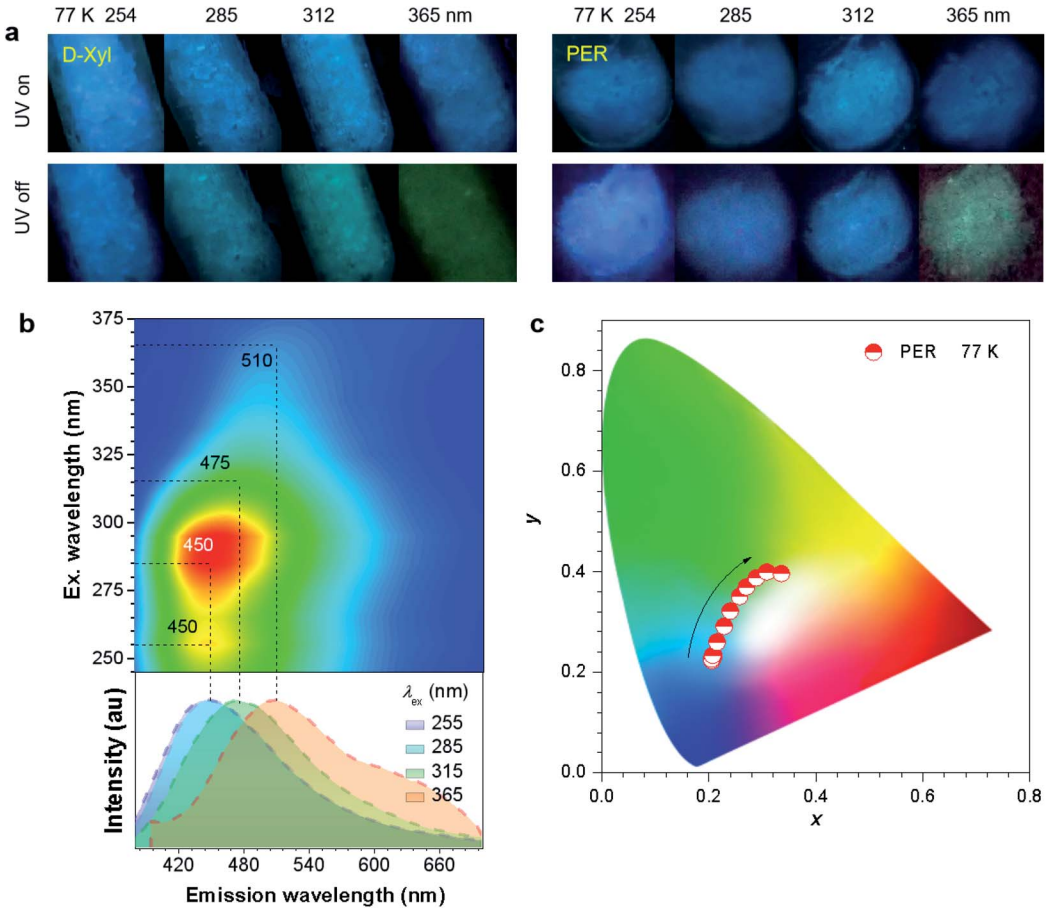


Fig. 4 (a) Photographs of D-Xyl and PER crystals taken at 77 K under varying UV light wavelengths or after stopping the irradiation. (b) Excitation–phosphorescence mapping and the phosphorescence spectra with different excitations ($t_d$ = 0.1 ms) of PER crystals at 77 K. (c) Trajectory of phosphorescence colors of PER crystals at 77 K, recorded by the change in the $\lambda_{ex}$ from 245 to 375 nm, in the CIE coordinate diagram.

changes with increasing $\lambda_{ex}$, accompanying the color variation from whitish-green to greenish-yellow (Fig. 3e). The p-RTP colors are mainly concentrated in the green region, and this may explain why the tunability of these crystals is less obvious when compared to that of D-Xyl.

Similar to D-Xyl, there were abundant intra- and intermolecular O···O interactions (*i.e.*, 3.478 and 2.706 Å in PER) in the crystals of these luminophores (Fig. 3f, g and S16, S17, ESI†), which constituted a 3D through-space electronic communication network among the oxygen atoms, thereby resulting in diverse clustered chromophores with varying electron delocalization. It was worth noting, that regardless of the fact that the distance among the intramolecular oxygens (3.478 Å) was greater than the sum of the van der Waals (vdW) radii (3.04 Å) in the PER crystals, the calculation results clearly indicate the through-space electron delocalization among the intramolecular oxygens, particularly in the LUMO levels (Fig. S18, ESI†), and this was presumably because of the shortened distance in the excited states.[65] These interactions, together with O···H hydrogen bonds, H···H dihydrogen bonds and C···O short contacts (Fig. S19–S21, ESI†), collectively stiffen the oxygen clusters, thus enabling the noticeable p-RTP emissions. Taken together, because of the heterogeneous population of emissive clusters, tunable multicolor p-RTP can be achieved with adequatly rigidified conformations.

To further check the effect of cryogenic treatment on the tunability of phosphorescence, the PL emission of D-Xyl and PER crystals was investigated at 77 K. Both crystals exhibited intense blue PL upon irradiation with UV light from 254 to 365 nm (Fig. 4a). After the removal of the excitation, the crystals showed blue-shifted afterglows with much longer durations when compared to those under ambient conditions (Fig. 4, S22

Table 2 Summary of the $\lambda_{ex}$ and $\lambda_{em}$ ($t_d$ = 0.1 ms) of the crystals at room temperature (rt) and 77 K

| | D-Xyl | PER | D-Fru | D-Gal |
|---|---|---|---|---|
| $\lambda_{ex}$ [nm] | $\lambda_{em}$ [nm] | $\lambda_{em}$ [nm] | $\lambda_{em}$ [nm] | $\lambda_{em}$ [nm] |
| 255 (rt) | 435/475 | 500 | 410 | 425/495 |
| 285 (rt) | 510 | 505 | 515 | 505 |
| 315 (rt) | 525 | 520 | 535 | 510 |
| 255 (77 K) | 425/470 | 450 | — | — |
| 285 (77 K) | 475 | 450 | — | — |
| 315 (77 K) | 480 | 475 | — | — |

and Video S3, S4, ESI†). The tunable range of cryogenic phosphorescence was notably, extended into both much bluer and much redder areas (Fig. 4c and S22c, ESI†), which was proved from the blue-shifted peaks at the same $\lambda_{ex}$ (Table 2), which should be ascribed to the emission enhancement for such emissive species in frozen states. Taking PER crystals as an example, the emission colors of blue, blue, cyan and yellowish-green were noticed after stopping the UV light at wavelengths of 254, 285, 312 and 365 nm (Fig. 4a and Video S4, ESI†), respectively, whose emission spectra showed improved fractions in the blue region when compared with those at room temperature (Fig. 4b). These results indicate enhanced color tunability for the persistent phosphorescence of such non-conventional luminophores at 77 K and corroborate the presence of diverse emissive oxygen clusters in the crystals.

## Conclusions

In conclusion, a CTE strategy was proposed to achieve tunable multicolor persistent phosphorescence in non-conventional luminophores without any remarkable conjugates or even free of π segments, by virtue of the heterogeneous nature of the emissive clusters in these systems. The CTE strategy is proved effective, as demonstrated by a group of non-conventional luminophores comprising merely oxygen functionalities (–OH), *i.e.*, D-Xyl, PER, D-Fru and D-Gal. The clustering of oxygens created enriched energy levels and narrowed the energy gaps, thus promoting SOC and allowing the consequent ISC transitions. By taking advantage of multistate O···O communicating networks and effective intra- and inter-molecular interactions, heterogeneous oxygen clusters were constructed, further achieving p-RTP color tunability assisted by a rigid local environment. The strategy and results presented should encourage the rational design of single-component molecules with tunable p-RTP emission colors in a variety of applications in chemistry. Furthermore, these findings, in turn, offer more fundamental implications for the underlying mechanism of non-conventional luminophores.

## Conflicts of interest

There are no conflicts to declare.

## Acknowledgements

This work was financially supported by the National Natural Science Foundation of China (51822303) and the Medical-Engineering Cross Project of Shanghai Jiao Tong University (YG2016MS21).

## Notes and references

1 J. Lee, P. W. Bisso, R. L. Srinivas, J. J. Kim, A. J. Swiston and P. S. Doyle, *Nat. Mater.*, 2014, **13**, 524–529.
2 H. Lee, J. Kim, H. Kim, J. Kim and S. Kwon, *Nat. Mater.*, 2010, **9**, 745–749.
3 R. Deng, F. Qin, R. Chen, W. Huang, M. Hong and X. Liu, *Nat. Nanotechnol.*, 2015, **10**, 237–242.
4 L. Pan, S. Sun, A. Zhang, K. Jiang, L. Zhang, C. Dong, Q. Huang, A. Wu and H. Lin, *Adv. Mater.*, 2015, **27**, 7782–7787.
5 Y. P. Sun, B. Zhou, Y. Lin, W. Wang, K. A. S. Fernando, P. Pathak, M. J. Meziani, B. A. Harruff, X. Wang, H. Wang, P. G. Luo, H. Yang, M. E. Kose, B. Chen, L. M. Veca and S. Y. Xie, *J. Am. Chem. Soc.*, 2006, **128**, 7756–7757.
6 O. Chen, D. E. Shelby, Y. Yang, J. Zhuang, T. Wang, C. Niu, N. Omenetto and Y. C. Cao, *Angew. Chem., Int. Ed.*, 2010, **49**, 10132–10135.
7 Y. Sagara, S. Yamane, M. Mitani, C. Weder and T. Kato, *Adv. Mater.*, 2016, **28**, 1073–1095.
8 Z. Chi, X. Zhang, B. Xu, X. Zhou, C. Ma, Y. Zhang, S. Liu and J. Xu, *Chem. Soc. Rev.*, 2012, **41**, 3878–3896.
9 K. M. Lee, W. Y. Cheng, C. Y. Chen, J. J. Shyue, C. C. Nieh, C. F. Chou, J. R. Lee, Y. Y. Lee, C. Y. Cheng, S. Y. Chang, T. C. Yang, M. C. Cheng and B. Y. Lin, *Nat. Commun.*, 2013, **4**, 1544.
10 M. J. Sun, Y. W. Zhong and J. Yao, *Angew. Chem., Int. Ed.*, 2018, **57**, 7820–7825.
11 M. Irie, T. Fulcaminato, K. Matsuda and S. Kobatake, *Chem. Rev.*, 2014, **114**, 12174–12277.
12 Z. Mao, Z. Yang, Y. Mu, Y. Zhang, Y. F. Wang, Z. Chi, C. C. Lo, S. Liu, A. Lien and J. Xu, *Angew. Chem., Int. Ed.*, 2015, **54**, 6270–6273.
13 T. H. Kim, K. S. Cho, E. K. Lee, S. J. Lee, J. Chae, J. W. Kim, D. H. Kim and J. Y. Kwon, *Nat. Photonics*, 2011, **5**, 176–182.
14 L. Gu, H. Shi, L. Bian, M. Gu, K. Ling, X. Wang, H. Ma, S. Cai, W. Ning, L. Fu, H. Wang, S. Wang, Y. Gao, W. Yao, F. Huo, Y. Tao, Z. An, X. Liu and W. Huang, *Nat. Photonics*, 2019, **13**, 406–411.
15 S. Cai, H. Ma, H. Shi, H. Wang, X. Wang, L. Xiao, W. Ye, K. Huang, X. Cao, N. Gan, C. Ma, M. Gu, L. Song, H. Xu, Y. Tao, C. Zhang, W. Yao, Z. An and W. Huang, *Nat. Commun.*, 2019, **10**, 4247.
16 H. Wang, H. Shi, W. Ye, X. Yao, Q. Wang, C. Dong, W. Jia, H. Ma, S. Cai, K. Huang, L. Fu, Y. Zhang, J. Zhi, L. Gu, Y. Zhao, Z. An and W. Huang, *Angew. Chem., Int. Ed.*, 2019, **58**, 18776–18782.
17 Y. Su, Y. Zhang, Z. Wang, W. Gao, P. Jia, D. Zhang, C. Yang, Y. Li and Y. Zhao, *Angew. Chem., Int. Ed.*, 2019, **58**, 1–6.
18 X. Dou, Q. Zhou, X. Chen, Y. Tan, X. He, P. Lu, K. Sui, B. Z. Tang, Y. Zhang and W. Z. Yuan, *Biomacromolecules*, 2018, **19**, 2014–2022.
19 Q. Zhou, Z. Wang, X. Dou, Y. Wang, S. Liu, Y. Zhang and W. Z. Yuan, *Mater. Chem. Front.*, 2019, **3**, 257–264.
20 Q. Wang, X. Dou, X. Chen, Z. Zhao, S. Wang, Y. Wang, K. Sui, Y. Tan, Y. Gong, Y. Zhang and W. Z. Yuan, *Angew. Chem., Int. Ed.*, 2019, **58**, 12667–12673.
21 W. Zhao, Z. He, J. W. Y. Lam, Q. Peng, H. Ma, Z. Shuai, G. Bai, J. Hao and B. Z. Tang, *Chem*, 2016, **1**, 592–602.
22 K. Narushima, Y. Kiyota, T. Mori, S. Hirata and M. Vacha, *Adv. Mater.*, 2019, **31**, 1807268.
23 Z. An, C. Zheng, Y. Tao, R. Chen, H. Shi, T. Chen, Z. Wang, H. Li, R. Deng, X. Liu and W. Huang, *Nat. Mater.*, 2015, **14**, 685–690.

 

24 R. Kabe and C. Adachi, *Nature*, 2017, **550**, 384–387.
25 S. Hirata, K. Totani, J. Zhang, T. Yamashita, H. Kaji, S. R. Marder, T. Watanabe and C. Adachi, *Adv. Funct. Mater.*, 2013, **23**, 3386–3397.
26 Y. Su, S. Z. F. Phua, Y. Li, X. Zhou, D. Jana, G. Liu, W. Q. Lim, W. K. Ong, C. Yang and Y. Zhao, *Sci. Adv.*, 2018, **4**, eaas9732.
27 S. Tao, S. Lu, Y. Geng, S. Zhu, S. A. T. Redfern, Y. Song, T. Feng, W. Xu and B. Yang, *Angew. Chem., Int. Ed.*, 2018, **57**, 2393–2398.
28 D. Li, F. Lu, J. Wang, W. Hu, X. M. Cao, X. Ma and H. Tian, *J. Am. Chem. Soc.*, 2018, **140**, 1916–1923.
29 Z. Yang, Z. Mao, X. Zhang, D. Ou, Y. Mu, Y. Zhang, C. Zhao, S. Liu, Z. Chi, J. Xu, Y. C. Wu, P. Y. Lu, A. Lien and M. R. Bryce, *Angew. Chem., Int. Ed.*, 2016, **55**, 2181–2185.
30 E. Lucenti, A. Forni, C. Botta, L. Carlucci, C. Giannini, D. Marinotto, A. Pavanello, A. Previtali, S. Righetto and E. Cariati, *Angew. Chem., Int. Ed.*, 2017, **56**, 16302–16307.
31 O. Bolton, K. Lee, H. J. Kim, K. Y. Lin and J. Kim, *Nat. Chem.*, 2011, **3**, 205–210.
32 G. Zhang, G. M. Palmer, M. W. Dewhirst and C. L. Fraser, *Nat. Mater.*, 2009, **8**, 747–751.
33 X. Chen, C. Xu, T. Wang, C. Zhou, J. Du, Z. Wang, H. Xu, T. Xie, G. Bi, J. Jiang, X. Zhang, J. N. Demas, C. O. Trindle, Y. Luo and G. Zhang, *Angew. Chem., Int. Ed.*, 2016, **55**, 9872–9876.
34 S. Xu, R. Chen, C. Zheng and W. Huang, *Adv. Mater.*, 2016, **28**, 9920–9940.
35 G. He, W. T. Delgado, D. J. Schatz, C. Merten, A. Mohammadpour, L. Mayr, M. J. Ferguson, R. McDonald, A. Brown, K. Shankar and E. Rivard, *Angew. Chem., Int. Ed.*, 2014, **53**, 4587–4591.
36 H. Wu, W. Chi, G. Baryshnikov, B. Wu, Y. Gong, D. Zheng, X. Li, Y. Zhao, X. Liu, H. Agren and L. Zhu, *Angew. Chem., Int. Ed.*, 2019, **58**, 4328–4333.
37 Z. He, H. Gao, S. Zhang, S. Zheng, Y. Wang, Z. Zhao, D. Ding, B. Yang, Y. Zhang and W. Z. Yuan, *Adv. Mater.*, 2019, **31**, 1807222.
38 Z.-Y. Zhang, Y. Chen and Y. Liu, *Angew. Chem., Int. Ed.*, 2019, **131**, 6089–6093.
39 X. Chen, W. Luo, H. Ma, Q. Peng, W. Z. Yuan and Y. Zhang, *Sci. China: Chem.*, 2018, **61**, 351–359.
40 L. Yuan, H. Yan, L. Bai, T. Bai, Y. Zhao, L. Wang and Y. Feng, *Macromol. Rapid Commun.*, 2018, **39**, 1800658.
41 C. Shang, N. Wei, H. Zhuo, Y. Shao, Q. Zhang, Z. Zhang and H. Wang, *J. Mater. Chem. C*, 2017, **5**, 8082–8090.
42 C. Hu, Y. Ru, Z. Guo, Z. Liu, J. Song, W. Song, X. Zhang and J. Qiao, *J. Mater. Chem. C*, 2019, **7**, 387–393.
43 Q. Zhou, B. Cao, C. Zhu, S. Xu, Y. Gong, W. Z. Yuan and Y. Zhang, *Small*, 2016, **12**, 6586–6592.
44 W. I. Lee, Y. Bae and A. J. Bard, *J. Am. Chem. Soc.*, 2004, **126**, 8358–8359.
45 D. Wang and T. Imae, *J. Am. Chem. Soc.*, 2004, **126**, 13204–13205.
46 H. Lu, L. Feng, S. Li, J. Zhang, H. Lu and S. Feng, *Macromolecules*, 2015, **48**, 476–482.
47 E. Zhao, J. W. Y. Lam, L. Meng, Y. Hong, H. Deng, G. Bai, X. Huang, J. Hao and B. Z. Tang, *Macromolecules*, 2015, **48**, 64–71.
48 R. B. Restani, P. I. Morgado, M. P. Ribeiro, I. J. Correia, A. Aguiar-Ricardo and V. D. B. Bonifácio, *Angew. Chem., Int. Ed.*, 2012, **51**, 5162–5165.
49 V. D. B. Bonifácio, V. G. Correia, M. G. Pinho, J. C. Lima and A. Aguiar-Ricardo, *Mater. Lett.*, 2012, **81**, 205–208.
50 Y. Gong, Y. Tan, J. Mei, Y. Zhang, W. Z. Yuan, Y. Zhang, J. Sun and B. Z. Tang, *Sci. China: Chem.*, 2013, **56**, 1178–1182.
51 M. Fang, J. Yang, X. Xiang, Y. Xie, Y. Dong, Q. Peng and Z. Li, *Mater. Chem. Front.*, 2018, **2**, 2124–2129.
52 Y. Wang, X. Bin, X. Chen, S. Zheng, Y. Zhang and W. Z. Yuan, *Macromol. Rapid Commun.*, 2018, **39**, 1800528.
53 W. Z. Yuan and Y. Zhang, *J. Polym. Sci., Part A: Polym. Chem.*, 2017, **55**, 560–574.
54 D. A. Tomalia, B. Klajnert-Maculewicz, K. A. M. Johnson, H. F. Brinkman, A. Janaszewska and D. M. Hedstrand, *Prog. Polym. Sci.*, 2018, **90**, 35–117.
55 H. Zhang, Z. Zhao, P. R. McGonigal, R. Ye, S. Liu, J. W. Y. Lam, R. T. K. Kwok, W. Z. Yuan, J. Xie, A. L. Rogach and B. Z. Tang, *Mater. Today*, 2020, **32**, 275–292.
56 J. I. Zink, G. E. Hardy and J. E. Sutton, *J. Phys. Chem. C*, 1976, **80**, 248–249.
57 F. G. Wick, *J. Opt. Soc. Am.*, 1940, **30**, 302–306.
58 J. Mei, N. L. C. Leung, R. T. K. Kwok, J. W. Y. Lam and B. Z. Tang, *Chem. Rev.*, 2015, **115**, 11718–11940.
59 M. Baroncini, G. Bergamini and P. Ceroni, *Chem. Commun.*, 2017, **53**, 2081–2093.
60 S. Hirata, *Adv. Opt. Mater.*, 2017, **5**, 1700116.
61 P. Long, Y. Feng, C. Cao, Y. Li, J. Han, S. Li, C. Peng, Z. Li and W. Feng, *Adv. Funct. Mater.*, 2018, **28**, 1800791.
62 J. Wang, Z. Chai, J. Wang, C. Wang, M. Han, Q. Liao, A. Huang, P. Lin, C. Li, Q. Li and Z. Li, *Angew. Chem., Int. Ed.*, 2019, **58**, 17297–17302.
63 W. Zhao, T. S. Cheung, N. Jiang, W. Huang, J. W. Y. Lam, X. Zhang, Z. He and B. Z. Tang, *Nat. Commun.*, 2019, **10**, 1595.
64 B. Zhou and D. Yan, *Adv. Funct. Mater.*, 2019, **29**, 1807599.
65 R. D. Pensack, R. J. Ashmore, A. L. Paoletta and G. D. Scholes, *J. Phys. Chem. C*, 2018, **122**, 21004–21017.